HHS Public Access

Author manuscript

Dev Biol. Author manuscript; available in PMC 2016 December 01.

Published in final edited form as:

Dev Biol. 2015 December 1; 408(1): 140–150. doi:10.1016/j.ydbio.2015.09.020.

MiR-302/367 regulate neural progenitor proliferation, differentiation, and survival in neurulation

Si-Lu Yang[1,*], **Mei Yang**[1,*], **Stephanie Herrlinger**[1], **Chen Liang**[1], **Fan Lai**[2], and **Jian-Fu Chen**[1,✝]

[1]Department of Genetics, Department of Biochemistry & Molecular Biology, University of Georgia, Athens, GA 30602

[2]Biochemistry & Molecular Biology, University of Miami, Miami, FL 33136

Abstract

How neural progenitor cell (NPC) behaviors are temporally controlled in early developing embryos remains undefined. The *in vivo* functions of microRNAs (miRNAs) in early mammalian development remain largely unknown. *Mir-302/367* is a miRNA cluster that encodes miR-367 and four miR-302 members (miR302a-d). We show that miR-302b is highly expressed in early neuroepithelium and its expression decline as development progresses. We generated a *mir-302/367* knockout mouse model and found that deletion of *mir-302/367* results in an early embryonic lethality and open neural tube defect (NTD). NPCs exhibit enhanced proliferation, precocious differentiation, and decreased cell survival in mutant embryos. Furthermore, we identified Fgf15, Cyclin D1, and D2 as direct targets of miR-302 in NPCs *in vivo*, and their expression is enhanced in mutant NPCs. Ectopic expression of Cyclin D1 and D2 increases NPC proliferation, while FGF19 (human ortholog of Fgf15) overexpression leads to an increase of NPC differentiation. Thus, these findings reveal essential roles of miR-302/367 in orchestrating gene expression and NPC behaviors in neurulation; they also point to miRNAs as critical genetic components associated with neural tube formation.

Keywords

MiR-302/367; neural progenitors; embryo development

The neural plate consists of predominantly neural progenitor cells (NPCs) during neurulation. The flat neural plate undergoes bending, bilateral lifting, folding, and fusion to

✝Correspondence: chen2014@uga.edu, (706) 542-3429 (phone).
*These authors contributed equally to this work

Author Contributions

S-L. Y., M.Y., L.C., F.L. and J-F. C. conceived and performed all experiments, S.H. helped with the manuscript writing, J-F.C. designed and interpreted the experiments and wrote the manuscript.

Financial Statement

The authors declare that there are no competing financial interests that might be perceived as affecting the objectivity of these studies.

finally generate the closed neural tube (Massarwa et al., 2014). The NPC cell behaviors, including proliferation, differentiation, and cell survival, need to be precisely controlled to coordinate this complex and highly dynamic morphological process of neural tube closure. Deregulation of these cell behaviors leads to open neural tube defects (NTDs), which are the second most common birth defects in humans and occurs in 1~2 in 1000 live births (Copp, 2005; Greene and Copp, 2014; Wilde et al., 2014). For instance, NPCs exhibit a high-dorsal and low-ventral gradient in proliferation rate during neural tube closure, whose disruption results in NTDs (Kim et al., 2007). Ectopic expression of Notch3 leads to increased numbers of NPCs in association with cranial NTD (Lardelli et al., 1996). Inactivation of Hes1 and Numb leads to precocious differentiation of NPCs and cranial neural tube defects (Ishibashi et al., 1995; Zhong et al., 2000). However, our mechanistic studies of NPC proliferation and differentiation in neurulation have mainly focused on signal transduction and transcriptional regulation (Copp, 2005; Greene and Copp, 2014; Wilde et al., 2014). The post-transcriptional regulation of NPC behaviors during neural tube closure remains largely unknown.

MicroRNAs (miRNAs) are a class of small non-coding RNAs regulating gene expression at post-transcriptional levels (Bartel, 2009). Because individual miRNAs can bind to multiple targets with distinct functions, miRNAs are ideal regulators to orchestrate multiple cellular behaviors during neurulation by regulating different targets. However, to date, knockout of individual or clusters of miRNAs mostly result in mild developmental phenotypes without disruption of early neurulation (Park et al., 2010; Vidigal and Ventura, 2015). Therefore, the importance of miRNA functions and action mechanisms during early embryo development remain unknown in the mammalian system. *Mir-302/367* is a miRNA cluster encoding miR-367 and additional four miR302 members (miR-302a-d). During mouse development, miR-302/367 start to be expressed in the embryonic region after implantation, and become restricted to the anterior neural tube by embryonic day 8.5 (E8.5) (Parchem et al., 2014; Pernaute et al., 2014). Studies from cultured cells suggest that the miR-302 family plays essential roles in pluripotency, differentiation, cell cycle progression, and apoptosis regulation in embryonic stem cells (ESCs) or primed pluripotent stem cells (Card et al., 2008; Pernaute et al., 2014; Rosa et al., 2009; Wang et al., 2008). However, the *in vivo* roles of *mir-302/367* and their functional mechanisms have not yet been determined.

Here, by depleting the whole *mir-302/367* loci in mice, we examined the functions of miR-302/367 in mammalian embryo development. Loss of miR-302/367 function results in neural tube defects (NTDs) and early embryonic lethality. We found that NPCs exhibit increased proliferation, premature differentiation, and decreased cell survival in mutant embryos. Fgf15 and Cyclin D1/D2 are identified as the *in vivo* targets of miR-302 in NPCs. Together, these studies suggest that miR-302/367 control different NPC behaviors by regulating these different targets during neurulation.

Results

Mir-302/367 deletion results in embryonic lethality and neural tube defects (NTDs) in mice

Mir-302/367 is a miRNA cluster encoding a miR-367 and four miR-302 members (miR302a-d) that share the same seed sequence (Fig. 1A, seed sequence is in red). Previous

studies have not yet determined the expression of miR-302 after E8.5 during mouse brain development (Parchem et al., 2014; Pernaute et al., 2014). We examined miR-302b expression using RNAs isolated from the cranial neuroepithelium of E9.5/E10.5 embryos and found that miR-302b expression is gradually reduced as development proceeds (Fig 1B). To assess *mir-302/367* functions in neural progenitor cells (NPCs) and embryo development, we generated *mir-302/367* mutant mice using gene trap embryonic stem (ES) cells in which the entire cluster of miRNA genes was removed (Fig. 1C). RT-PCR analysis confirmed that miR-302b is absent in E9.5 homozygous mutant neuroepithelium compared to controls (Fig. 1D). Further sequencing of mutant genomic DNA revealed the expected deletion of miR-302/367 loci (data not shown). Mir-302/367 is located in the intron flanked by exon 7 and 8 of gene *Larp7* in the mouse genome. RT-PCR analysis shows that *Larp7* mRNA expression is not significantly changed by the deletion of *mir-302/367* (Fig 1E), indicating the specificity of *mir-302/367* depletion in the knockout mouse.

Mir-302/367 heterozygous mice are viable, fertile, and have indistinguishable morphology from wild type littermates. We recovered homozygous mutant embryos from E8.5 to E11.5 with expected Mendelian frequency, but were unable to obtain homozygous mutants at E13.5 or E18.5 (Fig. 1F), suggesting that *mir-302/367* depletion results in an embryonic lethal phenotype around E12.5. We did not find obvious morphological abnormalities of mutant embryos before E9.5 (Fig. 2A). E11.5 mutant embryos exhibit severe NTDs (Fig. 2B). Our analysis at E10.5 shows that the majority of mutant embryos (85%) exhibit open neural tube defects (NTDs) at the cranial region (Fig. 2C, D), whereas some mutant embryos have closed neural tubes (Fig. 2E). Analysis of crown to rump length suggests that mutant embryos are reduced in size compared with controls (Fig. 2D–F). Together, these data suggest that *mir-302/367* is required for proper neural tube formation and embryo survival around mid-gestation.

Loss of *mir-302/367* results in an increase in proliferation and differentiation of neural progenitor cells (NPCs)

Sonic hedgehog (Shh) signaling and Bone morphogenetic protein (Bmp) signaling function together to regulate transcriptional networks to pattern the neural tube along the dorsal-ventral (DV) axis (Briscoe et al., 2000; Jessell and Dodd, 1990). To examine if there is a DV patterning defect in the *mir-302/367* mutant embryos, we examined the expression of markers reflective of the distinct positions of NPCs along the DV axis of the neural tube, including Msx1/2, Pax3, Pax6, Nkx2.2, and Shh for dorsal, intermediate, and ventral neural tube, respectively. In E9.5 mutant embryos, the spatial distribution of these patterning markers resembled those seen in littermate controls (Supplemental Fig. 1), suggesting that DV patterning is not disrupted in the *mir-302/367* mutant embryos.

To begin to understand the potential cellular defects in *mir-302/367* mutant embryos, we examined NPCs at E8.5 and found that there is a significant increase of NPC numbers in mutant neural tubes compared to controls (Fig. 2G–I). To ask if cell proliferation rate is altered in the *mir-302/367* mutants, we firstly examined mitotic NPCs in cranial neural tubes using phospho-histone H3 (p-H3) antibodies. In E8.5/E9.5 wild type embryos, the p-H3 positive NPCs are lined along the ventricular surface of the neuroepithelium (Fig. 3A, B).

We found that there is a significant increase of p-H3 positive cells in the mutants compared to controls (Fig. 3A–C). Since p-H3 only labels cells in the M phase, we examined cells in S phase by performing 0.5 hr 5-ethynyl-2′-deoxyuridine (EdU) labeling experiments. In wild type embryos a significant portion of the ventricular zone of the neuroepithelium is free of EdU-positive cells (Fig. 3D). In contrast, the majority of the neuroepithelium zone is occupied by EdU-positive cells in the mutants (Fig. 3E). Statistical analyses suggest that *mir-302/367* depletion results in a significant increase in EdU-positive NPCs in the mutants compared to controls (Fig. 3F). Together, p-H3 immunostaining and EdU labeling studies suggest that there is an increase in NPC proliferation rate in the mutant embryos compared to controls.

To ask if differentiation is altered in mutant NPCs, we analyzed the generation of motor neurons, which differentiate early in the ventral spinal cord and are labeled by Isl1/2 (Pfaff et al., 1996). Immunostaining results show that there is a significant increase in differentiated motor neurons in the mutant embryos compared to controls (Fig. 3G–I). Furthermore, we used Neurofilament (NF) and TuJ1 antibodies to mark differentiated neurons. Whereas NF/TuJ1 staining are barely detected in cranial regions of both E8.5 wild type and mutant embryos, we detected an increase of NF staining in the spinal cord of E8.5 mutant embryos (Supplemental Fig. 2A). Somite-matched E9.5 embryos at comparable anterior-posterior levels within neural tubes showed a significant increase in NF staining in the mutants compared to controls (Supplemental Fig. 2B, C), suggesting a premature differentiation of mutant NPCs. To ask whether or not these premature differentiated NPCs exit the cell cycle, we used Ki67 to label NPCs in all cell cycle phases except G0 and TuJ1 to mark differentiated neurons. We found that there is a significant increase in TuJ1-positive cells in mutant neural tubes; some mutant cells express both Ki67 and TuJ1 (Supplemental Fig. 2D–F).Together, these data suggest that loss of *miR-302/367* leads to precocious neural differentiation of NPCs.

Loss of *mir-302/367* results in apoptotic cell death of neural progenitor cells (NPC)

Programmed cell death occurs in the central nervous system (CNS) during normal development (Kuan et al., 2000), and rapidly proliferating cells have highly sensitive apoptotic programs in early embryo formation (Pernaute et al., 2014). Therefore, we hypothesized that there is an increased cell death in the mutant NPCs. To test this hypothesis, we performed TUNEL staining on sections from E10.5 hindbrain regions and found a drastic increase in TUNEL-positive cells in the mutants (Fig. 4A, B). We also detected an increase in cell death in the spinal cords of E10.5 mutant embryos (Supplemental Fig. 3A–C). Interestingly, the increased cell death is restricted to the neural tube areas since we failed to detect a significant change of TUNEL-positive cells in non-neural tube areas in the mutants compared to controls (Supplemental Fig. 3A–B, D). To ask if this cell death defect occurs before the manifestation of morphological abnormalities, we performed TUNEL analysis on E8.5 embryo sections at cranial regions and did not find a significant difference between wild type (WT) and mutants (Fig. 4C, D). Next we examined E9.5 neural tubes and found a significant increase in TUNEL-positive cells in mutants at both hindbrain and spinal cord regions (Fig. 4E–G). Since TUNEL assay detects the final step of apoptotic cell death, we used activated Caspase 3 antibodies to examine the early

events of programmed cell death. Consistently, we found a significant increase in Caspase 3-positive cells in the neural tubes of mutant embryos (Supplemental Fig. 3E–G). Together, these data suggest that *mir-302/367* depletion results in a significant increase in cell death.

MiR-302/367 regulate the expression of Cyclin D1 and D2 in neural progenitor cells (NPCs)

In response to mitogenic signals, D-type cyclins, including Cyclin D1 and Cyclin D2, drive the early to mid-G1 phase of cell cycle progression (Massagué, 2004). Independent studies have shown that miR-302 directly targets Cyclin D1 by binding to its 3′-UTR in human embryonic stem (ES) cells or cancer cells (Card et al., 2008; Yan et al., 2014). The 3′UTRs of Cyclin D1/D2 both contain miR-302 binding sites (http://www.targetscan.org). Therefore, we hypothesized that Cyclin D1/D2 are direct targets of miR-302 in NPCs *in vivo*. To test this hypothesis, we performed *in situ* hybridization studies. Mammalian miRNAs repress gene expression by destabilizing target mRNA expression (Guo et al., 2010); loss of miRNA function is predicted to result in upregulation of its target mRNAs. We detected a visible increase in Cyclin D1 and D2 mRNA in cranial regions of E8.5 mutant neural tubes (Fig. 5A, C). Because morphologies are disrupted in the E9.5 cranial neural tubes of mutant embryos, we further performed in situ hybridization analyses on spinal cord sections. We found a visible increase in Cyclin D1 and D2 mRNA expression in the mutant neural tubes compared to controls (Fig. 5B, D). Interestingly the upregulated Cyclin D1/D2 mRNA is preferentially localized to the dorsal portion of the neural tube (Fig. 5B, D); spatial localization of Cyclin D1 in mutant spinal cord is confirmed by immunostaining analysis (Fig. 5E).

To quantify the upregulation of Cyclin D1/D2 protein in mutant embryos, we performed western blot analyses using lysates from E9.5 neuroepithelium. We found a significant increase in Cyclin D1/D2 protein levels in the mutant cranial neuroepithelium compared with controls (Fig. 5F, G). These data suggest that the expression of Cyclin D1/D2 is increased at both mRNA and protein levels in the *mir-302/367* mutants. MiRNAs destabilize target mRNAs by binding to their 3′-UTRs (Bartel, 2009). We confirmed the miR-302 binding site in the 3′-UTR of Cyclin D1 and D2 (Fig. 5H). To examine if the 3′-UTRs of Cyclin D1 and D2 respond to the ectopic expression of miR-302 in a miR-302 binding site-dependent manner, we performed a luciferase reporter assay. The experimental results show that miR-302b repressed the luciferase reporter activities of 3′-UTRs of Cyclin D1 and D2 in a dosage-dependent manner, whereas mutations in the predicted binding sites of miR-302b significantly prevented this repression (Fig. 5I, J). Together, these data suggest that Cyclin D1/D2 are the bona fide targets of miR-302 and miR-302/367 repress the expression of Cyclin D1/D2 *in vivo*, which is consistent with our evidence that depletion of miR-302/367 leads to an increase in NPC proliferation.

MiR-302/367 regulate the expression of Fgf15 in neural progenitor cells (NPCs)

MiR-302 functions together with the RNA binding protein Lin41/Trim71 to regulate embryonic stem (ES) cell self-renewal (Chang et al., 2012). Previously, we showed that Lin41 regulates Fgf signaling to control the balance of proliferation and differentiation of NPCs (Chen et al., 2012). Therefore we hypothesized that miR-302/367 regulates Fgf signaling. To test this hypothesis, we examined Fgfr1 and Fgfr2 expression levels using

lysates isolated from E9.5 cranial neuroepithelium. Western blot analyses show that there is no significant difference in protein expression of Fgfr1 and Fgfr2 between wild type and mutant embryos (Supplemental Fig. 4B, C). During early neural development, there are four Fgf ligands that are predominantly expressed in the cranial neural tube area, including Fgf8, Fgf15, Fgf17, and Fgf18 (Bachler and Neubüser, 2001; Borello et al., 2008; Crossley and Martin, 1995). To ask if these Fgf signaling ligands have altered expression patterns in mutant neural tubes, we performed RT-PCR analyses. We found that Fgf15 mRNA is significantly increased in the mutant cranial neuroepithelium compared to controls, but not Fgf8, Fgf17, or Fgf18 (Fig. 6A). In situ hybridization analysis detected a visible increase in Fgf15 mRNA in mutant embryos at both E8.5 and E9.5 stages (Fig. 6B, C). In contrast, we did not detect such changes in mRNA expression of other genes, including *Fgf17*, *Fgf18*, *Foxd3*, *Brachyury*, and *Twist* (Supplemental Fig. 4D–H), suggesting the specificity of Fgf15 upregulation in mutant embryos. To ask if Fgf15 protein is also upregulated in mutant embryos, we performed western blot analyses using E9.5 cranial neuroepithelium. The experimental results showed upregulation of Fgf15 and not Fgf8 protein in the mutant embryos (Fig. 6D, E). Together, these data suggest that miR-302/367 repress the expression of Fgf15 during early neural development.

So far our experimental evidence suggests that miR-302/367 is required for repressing the expression of Fgf15 and Cyclin D1/D2. Next we asked if miR-302 alone is sufficient to repress these target genes' expression. We performed a miR-302b gain-of-function study in neural progenitor NE-4C cells, a cell line established from the cerebral vesicle of E9.0 mouse embryos and used to study NPC proliferation and differentiation *in vitro* (Varga et al., 2008). We found that overexpression of miR-302b significantly reduces the protein levels of Fgf15 and Cyclin D1/D2 in the NE-4C cells (Fig. 6F, G). Together, these data suggest that miR-302 is necessary and sufficient to repress the expression of Cyclin D1/D2 and Fgf15. The Fgf15 3′-UTR contains a binding site for miR-302 (Fig. 6H). To ask if miR-302 represses Fgf15 3′UTR activity in a miR-302 binding site-dependent manner, we performed a luciferase reporter assay. We found that miR-302b represses the luciferase reporter activity of the Fgf15 3′UTR, whereas mutations in the miR-302 binding site significantly blocked the repression (Fig. 6I). Together, these data suggest that Fgf15 is a direct target of miR-302 *in vivo*, and miR-302/367 represses the expression of Fgf15 in NPCs during neural tube closure.

Ectopic expression of Cyclin D1/D2 and Fgf15 results in enhanced proliferation and differentiation of neural progenitor cells (NPCs) in vitro, respectively

To examine the biological significance of Cyclin D1/D2 upregulation in the *mir-302/367* mutant NPCs, we overexpressed Cyclin D1 or D2 in the NE-4C cells followed by EdU pulse labeling studies. Consistent with the well-established roles of Cyclin D1/D2 in promoting cell cycle progression (Lange et al., 2009; Massagué, 2004), their ectopic expression in NE-4C cells significantly enhanced cell proliferation compared to control treatment (Fig. 7A, B). These data, together with the observed enhanced NPC proliferation (Fig. 3) and increased Cyclin D1/D2 expression in mutant NPCs (Fig. 5), indicate that the increased NPC proliferation in the *mir-302/367* mutant neural tubes could be due to, at least in part, the upregulation of Cyclin D1/D2 expression.

Previous mouse genetic studies suggest that Fgf15 promotes neural differentiation (Borello et al., 2008). To ask if upregulation of Fgf15 in mutant NPCs could contribute to their premature differentiation *in vitro*, we attempted to examine the effects of Fgf15 overexpression on neural differentiation in NE-4C cells. Because of the technical challenge of purifying the functional recombinant protein of Fgf15, we instead used its human ortholog protein FGF19, which has been shown to function indistinguishably from mouse Fgf15 (Borello et al., 2008). Whereas it cannot directly induce neural differentiation of NE-4C cells, FGF19 significantly promotes retinoic acid (RA)-mediated neural differentiation of NE-4C cells (Fig. 7C–E). These data, together with premature differentiation of mutant NPCs (Fig. 3, Supplemental Fig. 2) and Fgf15 upregulation in mutant NPCs (Fig. 6), indicate that premature differentiation of mutant NPCs could be due to, at least in part, the upregulation of Fgf15 expression in the mutant neural tubes.

Discussion

Here we identified miR-302/367 as a novel gene regulator at post-transcriptional levels, which is required for mammalian neural tube formation and embryo survival. MiR-302/367 regulate neural progenitor cell (NPC) proliferation, differentiation, and survival in early developing embryos. They do so through, at least in part, repressing different miRNA targets including Cyclin D1/D2 and Fgf15 (Fig. 7F).

MiR-302/367 *in vivo* functions

The importance of global miRNA function in mouse embryo development is highlighted by early embryonic lethal phenotypes associated with deletions of miRNA biogenesis genes, such as *Dicer*, *Dgcr8*, and *Ago2* (Bernstein et al., 2003; Morita et al., 2007; Wang et al., 2007). However, depletion of individual or clustered miRNAs in mice largely results in mild phenotypes without fully penetrant embryonic lethality (Park et al., 2010; Vidigal and Ventura, 2015). Similar studies find that individual or most families of *C. elegans* miRNAs are not essential for development and viability (Alvarez-Saavedra and Horvitz, 2010; Miska et al., 2007). A central paradigm that has emerged is that miRNAs generally fine-tune gene expression and provide the robustness for biological processes (Ebert and Sharp, 2012; Leung and Sharp, 2010; Mendell and Olson, 2012). Therefore, whether individual miRNAs or miRNA clusters play essential roles in early mammalian development remains an open question. Here our mouse genetic studies on miR-302/367 provide the evidences that miRNAs functions are essential for early mammalian embryo development; miRNAs play decisive roles in early development including determining progenitor cell proliferation or differentiation and their survival or death.

Mir-302/367 cellular functions remain unclear based on cell culture studies *in vitro*. It has been reported that miR-302/367 promote G1/S phase transitions in embryonic stem (ES) cells (Card et al., 2008; Wang et al., 2008). Recent studies also showed that miR-302 inhibits cell proliferation and function as tumor suppressors in various cancer cell lines (Jamshidi-Adegani et al., 2014; Wang et al., 2013; Yan et al., 2014). Here we provided genetic evidences that miR-302/367 inhibit NPC proliferation during early brain development, at least in part, by repressing the expression of Cyclin D1/D2 (Fig. 3, 5). In

addition, our studies revealed that miR-302/367 prevents precocious differentiation of NPCs through, at least in part, repressing pro-differentiation factor Fgf15 (Fig. 3, 6, Supplemental Fig. 2). Therefore, we identified a novel function and action mechanism of miR-302/367 in regulating NPC differentiation. Recent studies from primed pluripotent stem cells suggest that miR-302, together with other miRNAs, control the apoptotic threshold by repressing proapoptotic protein Bim (Pernaute et al., 2014). These intriguing data raise the possibility that miR-302/367 regulate cell death through repressing Bim in NPCs. Our RT-PCR analysis failed to detect a difference in Bim mRNA expression between wild type and mutant neuroepithelium (Supplemental Fig. 4A). However, Bim dysregulation could occur in specific areas at certain developmental stages, and future studies should examine the temporal-spatial expression of Bim in the *mir-302/367* mutant embryos. Since miR-367 has distinct seed sequence with miR-302, it is likely that miR-367 has different targets and distinct functions with miR-302. To tease apart miR-302 and miR-367 functions, future studies could examine if and which cellular defects could be rescued by ectopic expression of miR-302 or miR-367 in the mutant background. Because mammalian miRNAs destabilize their target mRNAs (Bartel, 2009; Guo et al., 2010), future studies should also compare the transcriptome between wild type and mutant embryos coupled with bioinformatic analysis to identify additional miR-302/367 functional targets.

MiR-302/367 and neural tube defects (NTDs)

More than 200 NTD causing genes have been identified in mice (Harris and Juriloff, 2010). Different genes tend to fall into distinct functional categories, and their mutations are associated with distinct primary cellular defects. For example, PCP (planar cell polarity) gene mutations result in a cell rearrangement defect (Wallingford, 2012); cilia gene mutations lead to deficiencies of Hedgehog signaling and neural patterning (Murdoch and Copp, 2010); Shroom3, Abl, or Mena have been implicated in the process of apical constriction (Fox and Peifer, 2007; Haigo et al., 2003; Roffers-Agarwal et al., 2008), although their mutations all result in NTDs. Distinctively, our *mir-302/367* mutants cause multiple cellular defects, including proliferation, differentiation, and cell survival deficiencies (Fig. 3, 4, Supplemental Fig. 2, 3). This phenomenon is likely explained by the unique features of miRNA-mediated gene regulation due to the ability of miRNA to bind to multiple targets with distinct functions. Indeed, miR-302 target Cyclin D1/D2 and Fgf15 have established roles in proliferation and neural differentiation, respectively (Borello et al., 2008; Lange et al., 2009; Massagué, 2004). Future studies should determine to what extent these different targets mediate corresponding cellular functions of miR-302/367 during neural tube formation.

Excessive proliferation and/or precocious differentiation of NPCs during neurulation could cause the NTDs. Loss of E2f1 rescues the NPC overexpression and neural tube defect in *Phactr4* mutant embryos (Kim et al., 2007), suggesting that excessive proliferation could play causative roles in NTDs. In our *mir-302/367* mutant embryos, we detected a significant increase in NPC proliferation and precocious differentiation (Fig. 3 and Supplemental Fig. 2). Although excessive proliferation and precocious differentiation of NPCs could be involved, our current studies cannot conclude that they are the causes of NTDs in *mir-302/367* mutants. Neural tube defects (NTDs) alone are not sufficient to cause

embryonic lethal phenotypes *in utero* (Copp, 1995). Further in-depth studies need to be performed to understand why *mir-302/367* depletion results in embryonic lethality. During the preparation of this manuscript, a similar study was published (Parchem et al., 2015), and revealed that miR-302 is required for neural tube closure and embryo survival, which is consistent with our findings. Whereas only miR-302 cluster is deleted in this published study, both miR-302 and miR-367 are removed in our mutants. We found a significant increase of cell death in the miR-302/367 mutant embryos, which was not reported in miR-302 null embryos (Parchem et al., 2015). Future studies should reveal if miR-367 is particularly essential for NPC survival and how it functions differently with miR-302 during early embryo development.

Materials and Methods

Generation of *mir-302/367* mutant mice

The ES cell line *mir-302/367* cluster 3N2 was obtained from the Mutant Mouse Regional Resource Center (MMRRC). The cluster of miRNAs was removed via homologous recombination by a LoxP-F3-PGK-EM7-PuroΔtk-bpA-LoxP-FRT targeting vector with 5′ and 3′ arms of homology. The Mouse Genetic Core Facility at National Jewish Health (NJH) at Colorado Denver performed ES cells injection into C57BL/6N blastocysts. The chimeric offspring were mated to 129S1/SvImJ mice for germline transmission; the germline transmitted heterozygous females were crossed with CMV-Cre males to remove the PGK/EM7:*puroΔtk* cassette (Fig. 1C). The PCR primers used for genotyping are: miR-302F: AATGCATCTCCTGGCTCTGT; miR-302R: AGGAGTTGCTCCCCAAAAAT.

EdU labeling

For 0.5 hour EdU pulse chase experiments in Figure 3D–E, E9.5 pregnant mice were injected intraperitoneally with EdU at 100 mg/kg of body weight. The animals were sacrificed 0.5 hr after the injection followed by EdU staining as described in the Click-iT EdU Imaging Kit (C10338, Invitrogen). The embryos were dissected out and fixed in 4% paraformaldehyde (PFA) at room temperature for 2hr, followed by incubation in 25% sucrose for 16 hour and embedded in the O.C.T. solution. The cryostat sections were prepared and processed as described above. EdU staining were detected by Click-iT® EdU Alex Fluor® Imaging Kit (C10338, Invitrogen). For EdU pulse labeling studies in Figure 7A–B, NE-4C cells plated with similar cell densities were transfected with control (EGFP), Cyclin D1 or Cyclin D2 constructs. 24 hours after transfection, cells were treated with 20 ug/mL EdU for 25 minutes before fixation for EdU detection.

Western blot analyses

Cranial neuroepithelium were micro-dissected from E9.5 wild type and mutant embryos, and lysed in lysis buffer (50mM Tris-HCl (pH7.4), 150mM NaCl, 1mM EDTA, 1% Triton X-100 and 1 tablet protease inhibitor (Roche) per 10ml). Cell debris was pelleted at 12500 rpm for 10 min at 4 degree and the supernatant was collected for analysis. For individual studies, the densitometry of individual blot signals from three independent western blot experiments were quantified using Image J software. The individual values for each blot

signal were normalized to respect to controls followed by the statistical analysis among different samples (Student's t-test). Western blots were performed using primary antibodies: TuJ1 (T3952, Sigma), β-actin (4970, Cell signaling), Fgf8 (MAB323, R& D system); Fgf15 (sc-16816, Santa Cruz); Cyclin D2 (sc-593, Santa Cruz), FgfR1 (ab10646, Abcam), FgfR2 (MAB7161, R&D system). Secondary antibodies used were goat anti-rabbit (172-1019, BioRad) and goat anti-mouse (172-1011, BioRad).

Quantitative RT-PCR

RNA was extracted using TRIzol (Invitrogen) using cranial neuroepithelium micro-dissected from embryos at different developmental stages. For regular RT-PCR to detect mRNA expression of Fgf8, Fgf15, Fgf17, Fgf18, Larp7, Bim (Fig. 1E, 6A, Supplemental Fig. 4A), the probes were ordered from Life Technologies. For miR-302b RT-PCR analyses (Fig. 1B, D), RNAs were extracted using Trizol and converted into cDNA with the TaqMan MicroRNA Reverse Transcription Kit (Applied Biosystems). Stem-loop RT primers for individual miRNAs will be used for RT reaction followed by the real-time PCR analysis, which allows quantitation of mature miRNA expression.

Cell culture and treatment with human FGF19

NE-4C cells were plated with similar densities in DMEM/10%FBS medium. After 16 hours, the medium was replaced with DMEM/0.5% FBS, and the cells were starved in DMEM/0.5% FBS for 24 hours before the treatment of hFGF19. In our assay, 0.1 ug/mL human FGF19 protein (969-FG-025, R&D systems) together with 5 ug/mL Heparin were added into NE-4C cells and cultured for 48 hours before protein lysate collection for Western blot analysis. Neural differentiation was induced with a 48 hours treatment with 10^{-6} M retinoic acid (RA, Sigma).

Supplementary Material

Refer to Web version on PubMed Central for supplementary material.

Acknowledgments

We thank our lab colleagues for stimulating discussions. We thank Dr. Jonathan Eggenschwiler for some *in situ* probe plasmids; and Dr. Nancy Manley, Brian Condie, Doug Menke, and James Lauderdale for using their equipment. We are grateful for the support of NICHD 5R00HD073269 (JC) and the work was supported in part by a University of Georgia start up fund.

References

Alvarez-Saavedra E, Horvitz HR. Many families of C. elegans microRNAs are not essential for development or viability. Curr Biol. 2010; 20:367–373. [PubMed: 20096582]

Bachler M, Neubüser A. Expression of members of the Fgf family and their receptors during midfacial development. Mech Dev. 2001; 100:313–316. [PubMed: 11165488]

Bartel DP. MicroRNAs: target recognition and regulatory functions. Cell. 2009; 136:215–233. [PubMed: 19167326]

Bernstein E, Kim SY, Carmell MA, Murchison EP, Alcorn H, Li MZ, Mills AA, Elledge SJ, Anderson KV, Hannon GJ. Dicer is essential for mouse development. Nat Genet. 2003; 35:215–217. [PubMed: 14528307]

Borello U, Cobos I, Long JE, McWhirter JR, Murre C, Rubenstein JLR. FGF15 promotes neurogenesis and opposes FGF8 function during neocortical development. Neural Dev. 2008; 3:17. [PubMed: 18625063]

Briscoe J, Pierani A, Jessell TM, Ericson J. A homeodomain protein code specifies progenitor cell identity and neuronal fate in the ventral neural tube. Cell. 2000; 101:435–445. [PubMed: 10830170]

Card DAG, Hebbar PB, Li L, Trotter KW, Komatsu Y, Mishina Y, Archer TK. Oct4/Sox2-regulated miR-302 targets cyclin D1 in human embryonic stem cells. Mol Cell Biol. 2008; 28:6426–6438. [PubMed: 18710938]

Chang HM, Martinez NJ, Thornton JE, Hagan JP, Nguyen KD, Gregory RI. Trim71 cooperates with microRNAs to repress Cdkn1a expression and promote embryonic stem cell proliferation. Nat Commun. 2012; 3:923. [PubMed: 22735451]

Chen J, Lai F, Niswander L. The ubiquitin ligase mLin41 temporally promotes neural progenitor cell maintenance through FGF signaling. Genes & Development. 2012; 26:803–815. [PubMed: 22508726]

Copp AJ. Death before birth: clues from gene knockouts and mutations. Trends Genet. 1995; 11:87–93. [PubMed: 7732578]

Copp AJ. Neurulation in the cranial region--normal and abnormal. J Anat. 2005; 207:623–635. [PubMed: 16313396]

Crossley PH, Martin GR. The mouse Fgf8 gene encodes a family of polypeptides and is expressed in regions that direct outgrowth and patterning in the developing embryo. Development. 1995; 121:439–451. [PubMed: 7768185]

Ebert MS, Sharp PA. Roles for microRNAs in conferring robustness to biological processes. Cell. 2012; 149:515–524. [PubMed: 22541426]

Fox DT, Peifer M. Abelson kinase (Abl) and RhoGEF2 regulate actin organization during cell constriction in Drosophila. Development. 2007; 134:567–578. [PubMed: 17202187]

Greene NDE, Copp AJ. Neural tube defects. Annu Rev Neurosci. 2014; 37:221–242. [PubMed: 25032496]

Guo H, Ingolia NT, Weissman JS, Bartel DP. Mammalian microRNAs predominantly act to decrease target mRNA levels. Nature. 2010; 466:835–840. [PubMed: 20703300]

Haigo SL, Hildebrand JD, Harland RM, Wallingford JB. Shroom induces apical constriction and is required for hingepoint formation during neural tube closure. Curr Biol. 2003; 13:2125–2137. [PubMed: 14680628]

Harris MJ, Juriloff DM. An update to the list of mouse mutants with neural tube closure defects and advances toward a complete genetic perspective of neural tube closure. Birth Defects Res Part A Clin Mol Teratol. 2010; 88:653–669. [PubMed: 20740593]

Ishibashi M, Ang SL, Shiota K, Nakanishi S, Kageyama R, Guillemot F. Targeted disruption of mammalian hairy and Enhancer of split homolog-1 (HES-1) leads to up-regulation of neural helix-loop-helix factors, premature neurogenesis, and severe neural tube defects. Genes & Development. 1995; 9:3136–3148. [PubMed: 8543157]

Jamshidi-Adegani F, Langroudi L, Shafiee A, Mohammadi-Sangcheshmeh A, Ardeshirylajimi A, Barzegar M, Azadmanesh K, Naderi M, Arefian E, Soleimani M. Mir-302 cluster exhibits tumor suppressor properties on human unrestricted somatic stem cells. Tumour Biol. 2014; 35:6657–6664. [PubMed: 24705778]

Jessell TM, Dodd J. Floor plate-derived signals and the control of neural cell pattern in vertebrates. Harvey Lect. 1990; 86:87–128. [PubMed: 2152141]

Kim TH, Goodman J, Anderson KV, Niswander L. Phactr4 regulates neural tube and optic fissure closure by controlling PP1-, Rb-, and E2F1-regulated cell-cycle progression. Dev Cell. 2007; 13:87–102. [PubMed: 17609112]

Kuan CY, Roth KA, Flavell RA, Rakic P. Mechanisms of programmed cell death in the developing brain. Trends in Neurosciences. 2000; 23:291–297. [PubMed: 10856938]

Lange C, Huttner WB, Calegari F. Cdk4/cyclinD1 overexpression in neural stem cells shortens G1, delays neurogenesis, and promotes the generation and expansion of basal progenitors. Cell Stem Cell. 2009; 5:320–331. [PubMed: 19733543]

Lardelli M, Williams R, Mitsiadis T, Lendahl U. Expression of the Notch 3 intracellular domain in mouse central nervous system progenitor cells is lethal and leads to disturbed neural tube development. Mech Dev. 1996; 59:177–190. [PubMed: 8951795]

Leung AKL, Sharp PA. MicroRNA functions in stress responses. Molecular Cell. 2010; 40:205–215. [PubMed: 20965416]

Massagué J. G1 cell-cycle control and cancer. Nature. 2004; 432:298–306. [PubMed: 15549091]

Massarwa R, Ray HJ, Niswander L. Morphogenetic movements in the neural plate and neural tube: mouse. Wiley Interdiscip Rev Dev Biol. 2014; 3:59–68. [PubMed: 24902834]

Mendell JT, Olson EN. MicroRNAs in stress signaling and human disease. Cell. 2012; 148:1172–1187. [PubMed: 22424228]

Miska EA, Alvarez-Saavedra E, Abbott AL, Lau NC, Hellman AB, McGonagle SM, Bartel DP, Ambros VR, Horvitz HR. Most Caenorhabditis elegans microRNAs are individually not essential for development or viability. PLoS Genet. 2007; 3:e215. [PubMed: 18085825]

Morita S, Horii T, Kimura M, Goto Y, Ochiya T, Hatada I. One Argonaute family member, Eif2c2 (Ago2), is essential for development and appears not to be involved in DNA methylation. Genomics. 2007; 89:687–696. [PubMed: 17418524]

Murdoch JN, Copp AJ. The relationship between sonic Hedgehog signaling, cilia, and neural tube defects. Birth Defects Res Part A Clin Mol Teratol. 2010; 88:633–652. [PubMed: 20544799]

Parchem RJ, Moore N, Fish JL, Parchem JG, Braga TT, Shenoy A, Oldham MC, Rubenstein JLR, Schneider RA, Blelloch R. miR-302 Is Required for Timing of Neural Differentiation, Neural Tube Closure, and Embryonic Viability. Cell Rep. 2015; 12:760–773. [PubMed: 26212322]

Parchem RJ, Ye J, Judson RL, LaRussa MF, Krishnakumar R, Blelloch A, Oldham MC, Blelloch R. Two miRNA clusters reveal alternative paths in late-stage reprogramming. Cell Stem Cell. 2014; 14:617–631. [PubMed: 24630794]

Park CY, Choi YS, McManus MT. Analysis of microRNA knockouts in mice. Hum Mol Genet. 2010; 19:R169–75. [PubMed: 20805106]

Pernaute B, Spruce T, Smith KM, Sánchez-Nieto JM, Manzanares M, Cobb B, Rodríguez TA. MicroRNAs control the apoptotic threshold in primed pluripotent stem cells through regulation of BIM. Genes & Development. 2014; 28:1873–1878. [PubMed: 25184675]

Pfaff SL, Mendelsohn M, Stewart CL, Edlund T, Jessell TM. Requirement for LIM homeobox gene Isl1 in motor neuron generation reveals a motor neuron-dependent step in interneuron differentiation. Cell. 1996; 84:309–320. [PubMed: 8565076]

Roffers-Agarwal J, Xanthos JB, Kragtorp KA, Miller JR. Enabled (Xena) regulates neural plate morphogenesis, apical constriction, and cellular adhesion required for neural tube closure in Xenopus. Developmental Biology. 2008; 314:393–403. [PubMed: 18201691]

Rosa A, Spagnoli FM, Brivanlou AH. The miR-430/427/302 family controls mesendodermal fate specification via species-specific target selection. Dev Cell. 2009; 16:517–527. [PubMed: 19386261]

Varga BV, Hádinger N, Gócza E, Dulberg V, Demeter K, Madarász E, Herberth B. Generation of diverse neuronal subtypes in cloned populations of stem-like cells. BMC Dev Biol. 2008; 8:89. [PubMed: 18808670]

Vidigal JA, Ventura A. The biological functions of miRNAs: lessons from in vivo studies. Trends Cell Biol. 2015; 25:137–147. [PubMed: 25484347]

Wallingford JB. Planar cell polarity and the developmental control of cell behavior in vertebrate embryos. Annu Rev Cell Dev Biol. 2012; 28:627–653. [PubMed: 22905955]

Wang L, Yao J, Shi X, Hu L, Li Z, Song T, Huang C. MicroRNA-302b suppresses cell proliferation by targeting EGFR in human hepatocellular carcinoma SMMC-7721 cells. BMC Cancer. 2013; 13:448. [PubMed: 24083596]

Wang Y, Baskerville S, Shenoy A, Babiarz JE, Baehner L, Blelloch R. Embryonic stem cell-specific microRNAs regulate the G1-S transition and promote rapid proliferation. Nat Genet. 2008; 40:1478–1483. [PubMed: 18978791]

Wang Y, Medvid R, Melton C, Jaenisch R, Blelloch R. DGCR8 is essential for microRNA biogenesis and silencing of embryonic stem cell self-renewal. Nat Genet. 2007; 39:380–385. [PubMed: 17259983]

Wilde JJ, Petersen JR, Niswander L. Genetic, Epigenetic, and Environmental Contributions to Neural Tube Closure. Annu Rev Genet. 2014; 48:141007180313005.

Yan G-J, Yu F, Wang B, Zhou H-J, Ge Q-Y, Su J, Hu Y-L, Sun H-X, Ding L-J. MicroRNA miR-302 inhibits the tumorigenicity of endometrial cancer cells by suppression of Cyclin D1 and CDK1. Cancer Lett. 2014; 345:39–47. [PubMed: 24333727]

Yang M, Yang SL, Herrlinger S, Liang C, Dzieciatkowska M, Hansen KC, Desai R, Nagy A, Niswander L, Moss EG, et al. Lin28 promotes the proliferative capacity of neural progenitor cells in brain development. Development. 2015; 142:1616–1627. [PubMed: 25922525]

Zhong W, Jiang MM, Schonemann MD, Meneses JJ, Pedersen RA, Jan LY, Jan YN. Mouse numb is an essential gene involved in cortical neurogenesis. Proc Natl Acad Sci USA. 2000; 97:6844–6849. [PubMed: 10841580]

Highlights

1. *MiR-302/367* is required for embryo survival. Knockout *mir-302/367* results in early embryo lethality;
2. MiR-302/367 regulate neural tube closure. Knockout *mir-302/367* leads to neural tube defects (NTDs);
3. MiR-302/367 regulate proliferation, differentiation, and survival of neural progenitor cells (NPCs);
4. Cyclin D1/D2 and Fgf15 are the *in vivo* targets of miR-302, and their expression is enhanced in *mir-302/367* mutant NPCs;
5. Ectopic expression of Cyclin D1/D2 increases NPC proliferation, and FGF19 (human ortholog of Fgf15) overexpression promotes NPC differentiation.

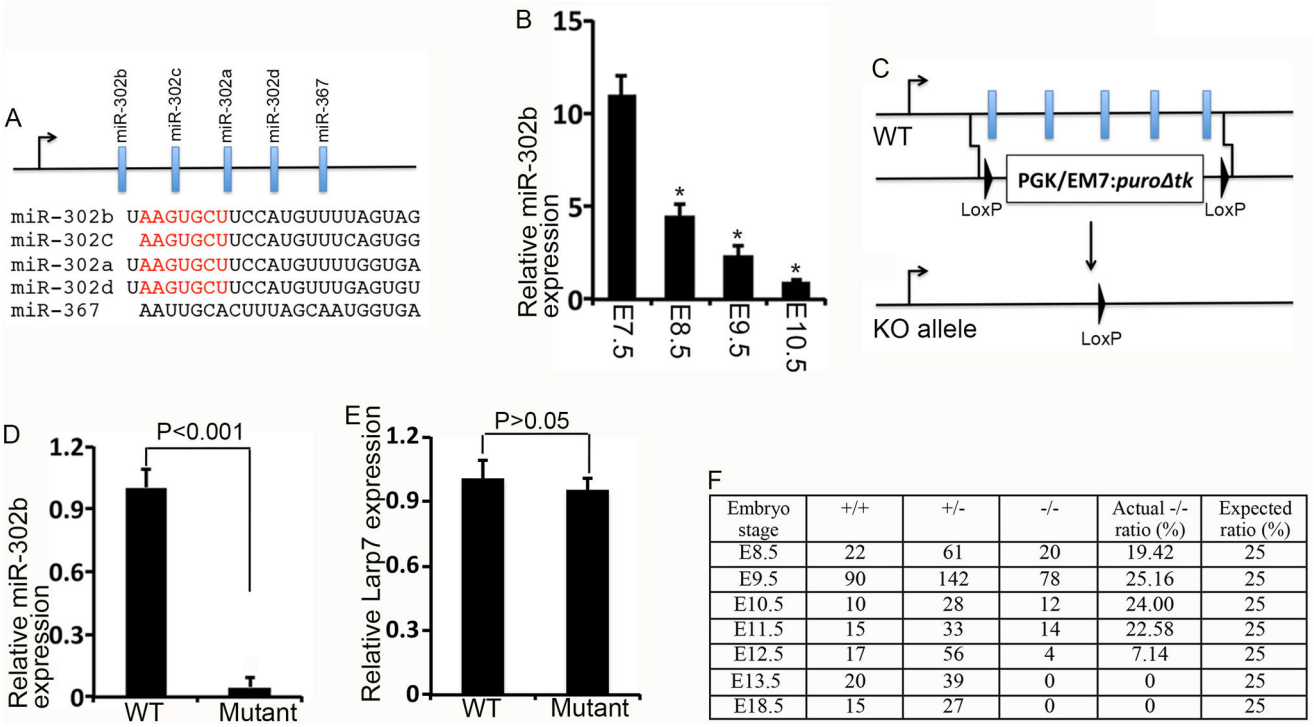

F

Embryo stage	+/+	+/-	-/-	Actual -/- ratio (%)	Expected ratio (%)
E8.5	22	61	20	19.42	25
E9.5	90	142	78	25.16	25
E10.5	10	28	12	24.00	25
E11.5	15	33	14	22.58	25
E12.5	17	56	4	7.14	25
E13.5	20	39	0	0	25
E18.5	15	27	0	0	25

Figure 1.

Loss of *mir-302/367* results in embryonic lethality in mice. (A) Diagram of the genomic structure of the *mir-302/367* locus on mouse chromosome 3. The red text highlights the common "seed sequences" among four members of miR-302 (miR-302a-d). (B) RT-PCR analysis of miR-302b expression using RNAs from E7.5/E8.5 embryos and cranial neuroepithelium of E9.5/E10.5 embryos. Error bars indicate SEM of data from three independent experiments using RNAs isolated from three different embryos at indicated stages. One way ANOVA analyses in conjunction with Tukey's test reveal significant differences between individual stages, *P<0.01. (C) Diagram of *mir-302/367* knockout strategy. The puromycin kinase fusion gene under control of PGK/EM7 promoter in the recombinant allele is removed by crossing with a CMV-Cre line. (D) RT-PCR analysis of miR-302b expression in the cranial neuroepithelium of E9.5 wild type and mutant embryos. Error bars indicate SEM of data from three independent measurements using RNAs isolated from three different embryos. P<0.001 (Student's t-test). (E) RT-PCR analysis of Larp7 mRNA expression using RNAs from E9.5 cranial neuroepithelium. Error bars indicate SEM of data from three independent measurements using RNAs from three different embryos. P>0.05 (Student's t-test), and difference is not significant. (F) Numbers of homozygous mutant embryos recovered from litters dissected at indicated embryonic stages. Chi-square analyses showed that the proportion of genotypes at E8.5 (P=0.167), E9.5 (P=0.211), E10.5 (P=0.644), and E11.5 (P=0.865) did not significantly differ from Mendelian expectations.

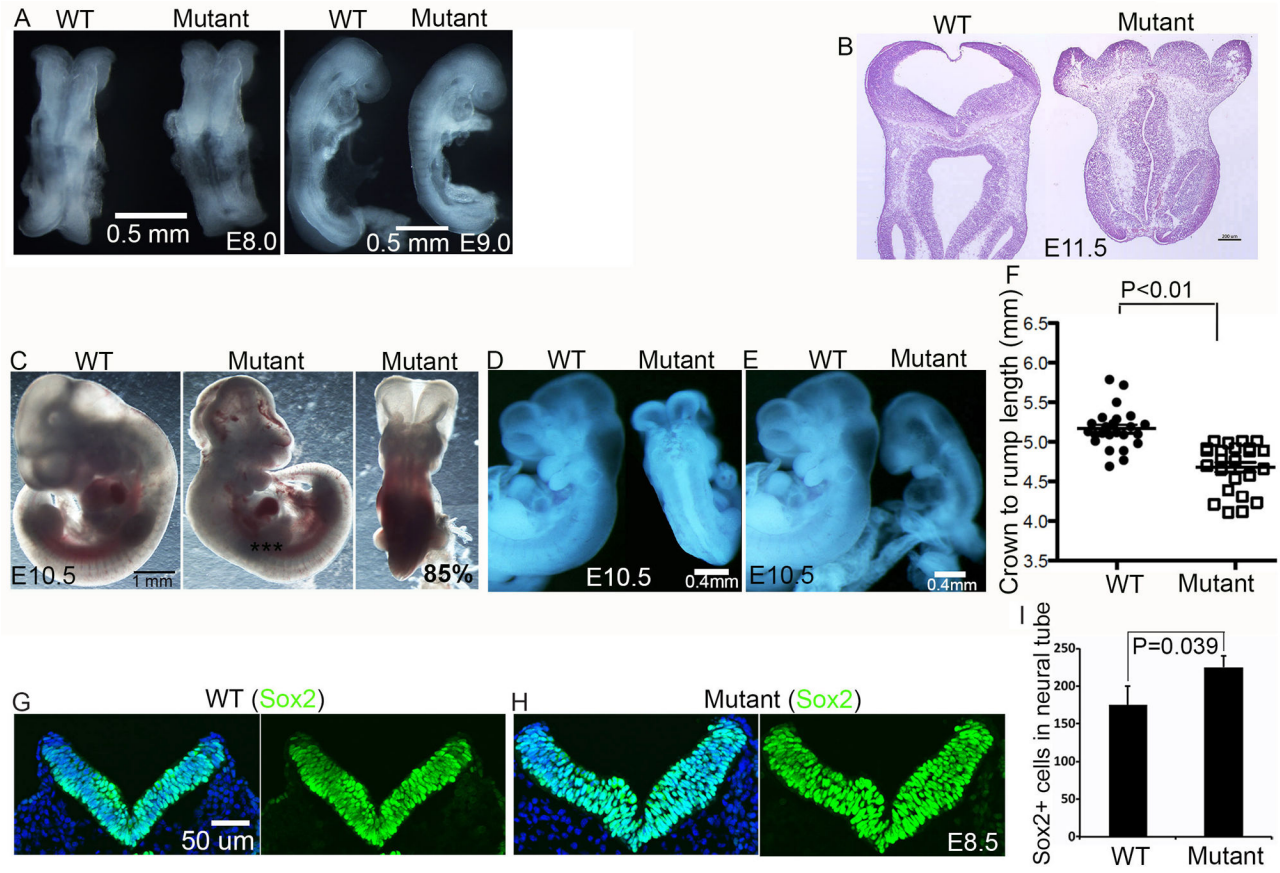

Figure 2.

Loss of *mir-302/367* results in neural tube defect (NTD) in mice. (A) Gross morphology of E7.5-8 wild type (WT) and mutant embryos. Scale bar: 0.5 mm. (B) H&E staining of transverse sections from E11.5 wild type and mutant neural tubes at comparable hindbrain regions. Scale bar: 200 um. (C) E10.5 homozygous mutant embryos exhibit open neural tube defects (NTDs) compared to littermate controls. Scale bar: 1 mm. (D) E10.5 homozygous mutant embryos exhibit open neural tube defects (NTDs) with reduced embryo size. Scale bar: 0.4 mm. (E) E10.5 homozygous mutant embryos exhibit reduced embryo size with closed neural tube. Scale bar: 0.4 mm. (F) Mutant embryos exhibit reduced crown to rump length (CRL) compared to littermate controls. A total 25 mutant embryos from 18 different litters at E10.5/E11.5 were measured under dissection microscopy, and 25 wild type embryos were used as controls. Data represent the SEM of 25 embryos for each genotype. $P<0.05$ (Student's t-test). (G, H) Confocal microscope images of E8.5 cranial sections stained with antibodies against Sox2. Hoechst stains nuclei (blue). Scale bar: 50 um. (I) Quantification of Sox2-positive cells in neural tube per section. Error bars represent SEM of 3 measurements from 3 embryos; 3 sections from each embryo were pooled for the analysis. *P=0.039 (Student's t-test).

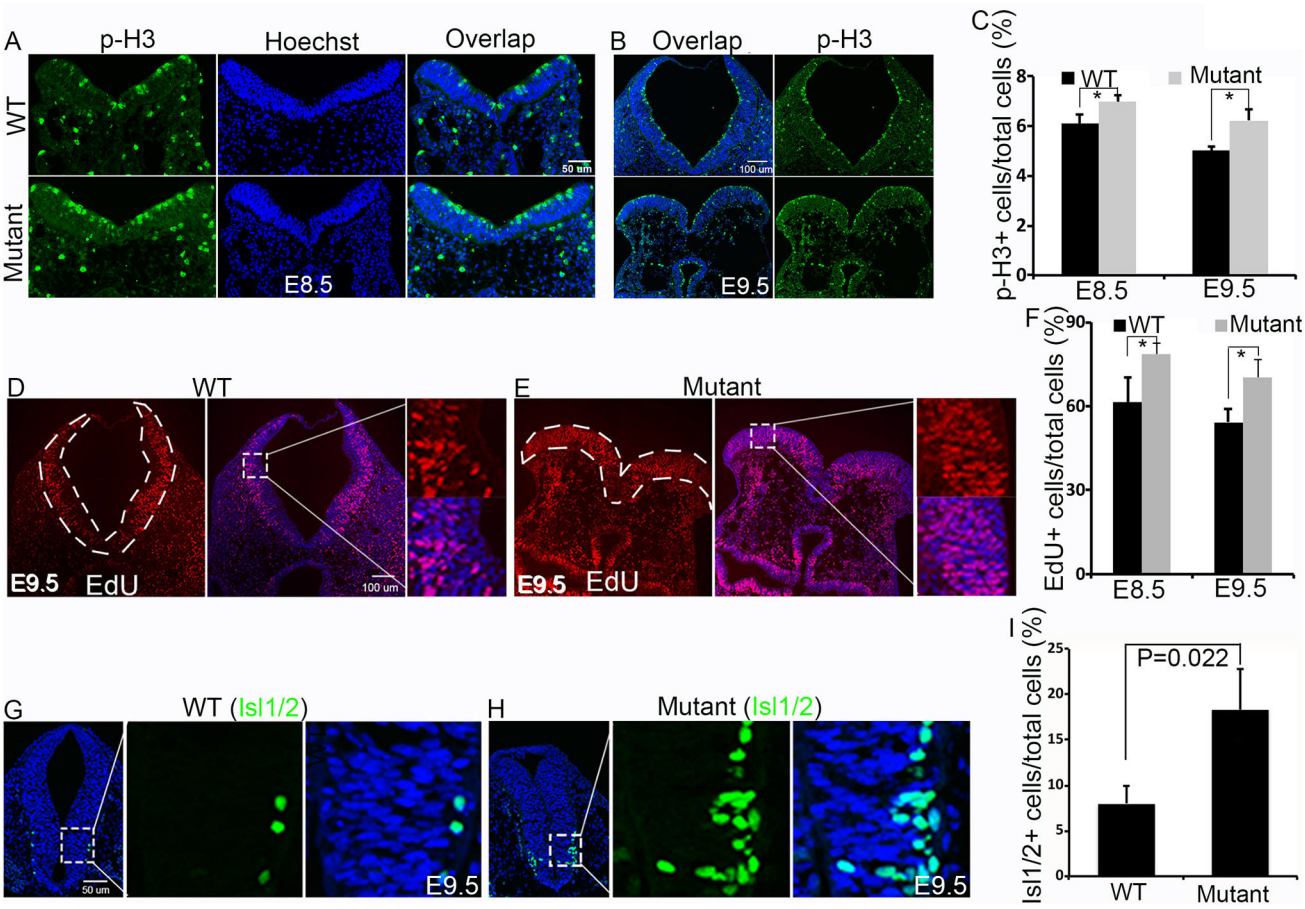

Figure 3.

Loss of *mir-302/367* results in an increase in proliferation and differentiation in neural progenitor cells (NPCs). (A, B) Confocal microscope images of hindbrain sections prepared from E8.5 (A) or E9.5 (B) embryos at comparable positions along rostral-caudal axis. Mitotic cells are labeled by p-H3 (green). Hoechst stains nuclei (blue). Scale bar: 50 um (A) and 100 um (B). (C) Quantification of percentage of p-H3 positive cells from total cells in neural tubes from experiment A and B. Error bars represent SEM of 3 measurements from 3 embryos; 3 sections from each embryo were pooled for the analysis. *P=0.027 (E8.5) and P=0.012 (E9.5) (Student's t-test); Two way ANOVA analysis did not detect a significant difference between stages. (D, E) Confocal microscope images of hindbrain sections at comparable positions along rostral-caudal axis derived from E9.5 wild type and mutant embryos after 0.5 hour EdU labeling. Individual dashed lines outline the neural tube area, and right panels represent the enlarged pictures from marked boxed areas in the middle panels. S phase cells are visualized by EdU-positive staining (red). Hoechst stains nuclei (blue). Scale bar: 100 um. (F) Quantification of the percentage of EdU-positive cells out of total neuroepithelial cells in the hindbrain sections in experiment D, E. Error bars indicate the SEM of 3 measurements from 3 embryos; 3 sections from each embryo were pooled for the analysis. *P=0.038 (E8.5) and *P=0.022 (E9.5) (Student's t-test); Two way ANOVA did not detect a significant difference between stages. (G, H) Confocal microscope images of spinal cord sections stained with antibodies against Isl1/2 (green) in E9.5 wild type and

mutant embryos. Hoechst stains nuclei (blue). Scale bar: 50 um. Right panels represent enlarged boxed areas (white) in the left panels. (I) Quantification of percentage of Isl1/2-positive cells out of total cells within a 4.73×10^4 um^2 field (white box area) in experiment G and H. Error bars represent SEM of 3 measurements from 3 embryos; 3 sections from each embryo were pooled for the analysis. P=0.022 (Student's t-test).

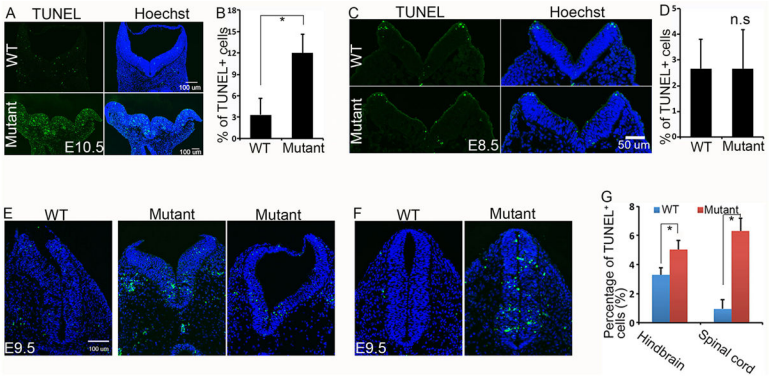

Figure 4.

Loss of *mir-302/367* results in apoptotic cell death of neural progenitor cells (NPCs). (A, C) TUNEL staining detects apoptotic cell death (green) in E10.5 (A) and E8.5 (C) wild type and mutant neural tubes in hindbrain regions. Note the drastic increase of TUNEL positive cells in the mutant sections compared to littermate controls at E10.5 but not at E8.5. Hoechst stains nuclei (blue). Scale bar: 100 um (A) and 50 um (C). (B, D) Quantitative measurement of TUNEL-positive cells from experiment A and C. The % of TUNEL-positive cells was calculated as the percentage of TUNEL-positive cells out of total number of neuroepithelial cells at each section. Error bars represent SEM of 3 measurements from 3 embryos; 3 sections from each embryo were pooled for the analysis. *P=0.008 (B) and n.s represents not significant (Student's t-test). (E, F) TUNEL staining detects apoptotic cell death (green) at E9.5 hindbrain (E) and spinal cord (F) regions. Scale bar: 100 um. (G) Quantification of TUNEL-positive cells out of total cells from experiment E and F. The TUNEL-positive percentage was calculated as the percentage of TUNEL-positive cells out of total number of neuroepithelial cells in neural tube. Error bars represent SEM of 3 measurements from 3 embryos; 3 sections from each embryo were pooled for the analysis. *P=0.021 and *P=0.003 (Student's t-test); Two way ANOVA detects a significant difference between hindbrain and spinal cord ($P<0.05$).

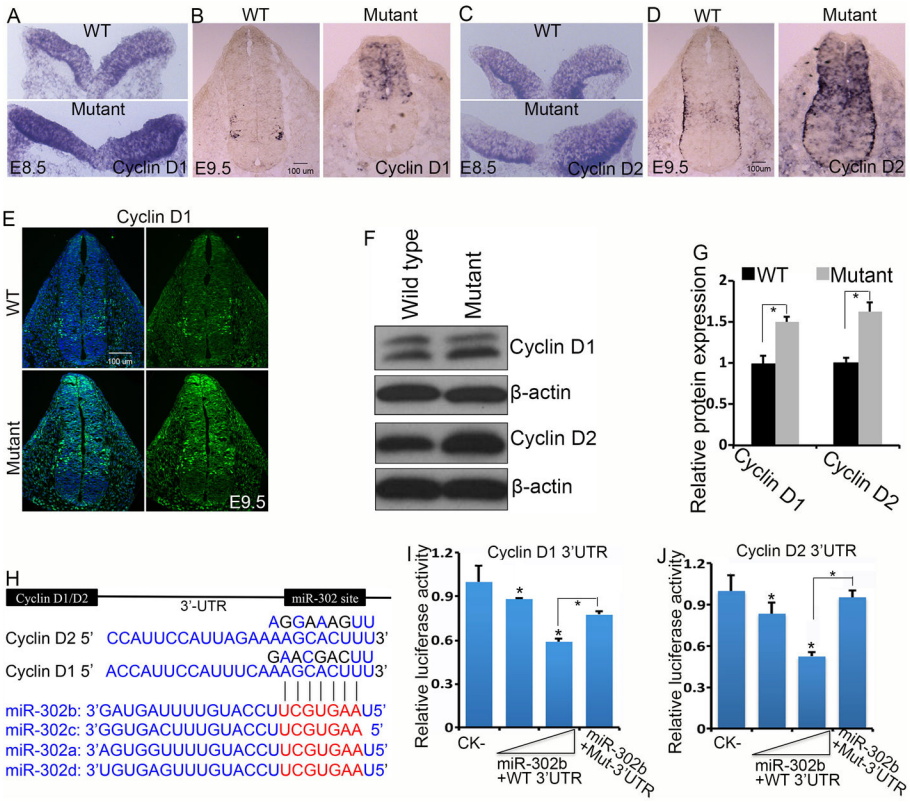

Figure 5.

MiR-302/367 regulate the expression of Cyclin D1/D2 in neural progenitor cells (NPCs). (A, B) Section in situ hybridization analysis detects Cyclin D1 mRNA expression at E8.5 cranial region (A) and E9.5 spinal cord region (B). Scale bar: 100 um. (C, D) Section in situ hybridization analysis detects Cyclin D2 mRNA expression at E8.5 cranial region (C) and E9.5 spinal cord region (D). Scale bar: 100 um. (E) Confocal microscope images of wild type and mutant sections stained with antibodies against Cyclin D1 (green). The sections were from comparable positions along the rostral-caudal axis of E9.5 spinal cord. Hoechst stains nuclei (blue). Scale bar: 100 um. (F) Western blot analysis of Cyclin D1 and D2 protein expression using lysates from E9.5 wild type and mutant cranial neuroepithelium. β-actin serves as the loading control. (G) Quantification of Western blot data from three independent blots in experiment F. The quantification was determined by densitometry and normalized to β-actin. *P<0.05 (Student's t-test). (H) Relative positions of miR-302 target sites in the 3′-UTR of Cyclin D1 and D2. Conserved seed region of miR-302a-d (2-8 nt from 5′ of miRNA) are shown in red text, and their alignment with the sequence from 3′-UTR of Cyclin D1/D2 is shown. Mutations in the 3′-UTR of Cyclin D1 and D2 (highlighted in black) were introduced to disrupt base-pairing between miR-302 seed sequence and 3′UTRs. (I, J) Luciferase reporter constructs containing wild type or mutated Cyclin D1 (I) or Cyclin D2 (J) 3′-UTR sequences were co-transfected with miR-302b mimics into NE-4C cells. 36 hours after transfection, the firefly luciferase activity was normalized to activity of Renilla. Error bars represent SEM of three replicates for each condition. One way ANOVA analysis in conjunction with Tukey's test was conducted (*P<0.05); the differences between lane 4 and lane 1 or 2 were not significant in both I and J.

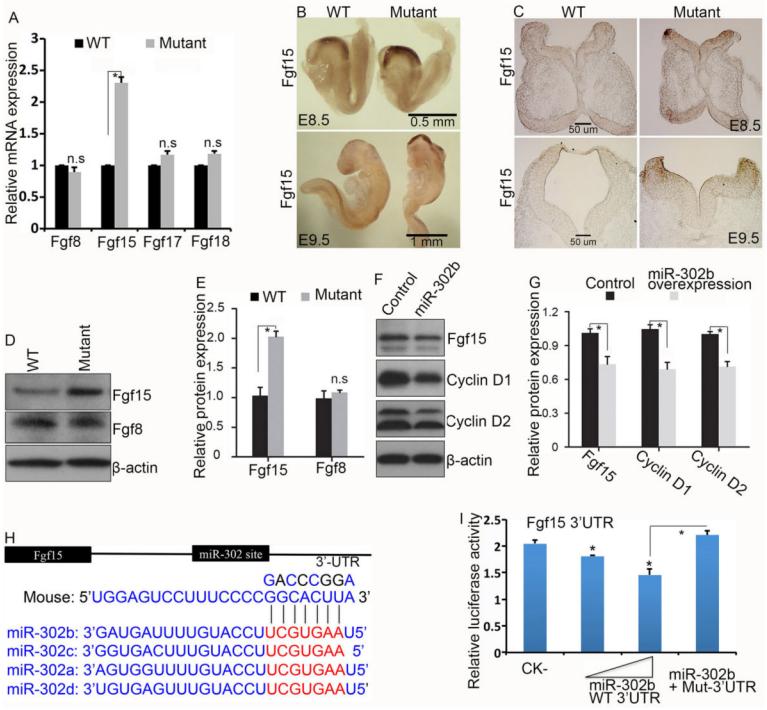

Figure 6.

MiR-302/367 regulate the expression of Fgf15 in neural progenitor cells (NPCs). (A) RT-PCR analysis of the mRNA expression of Fgf8, Fgf15, Fgf17 and Fgf18 using RNAs isolated from E9.5 wild type (WT) and mutant cranial neuroepithelium. Error bars represent SEM of results from three different embryos. N.s represents not significant, and *p<0.01 (Student's t-test). (B) Whole mount in situ hybridization of Fgf15 mRNA expression on E8.5 (upper panel) or E9.5 (lower panel) embryos. Scale bar: 0.5 mm (E8.5) and 1 mm (E9.5). (C) Coronal sections of embryos after Fgf15 whole mount in situ hybridization analyses in experiment B. Scale bar: 50 um. (D) Western blot analyses of protein expression of Fgf15 and Fgf8 using lysates from E9.5 wild type or mutant cranial neuroepithelium. (E) Quantification of Western blot data from three independent blots in experiment D. β-actin serves as a loading control. The quantification was determined by densitometry and normalized to β-actin; n.s indicates not significant, and *p< 0.01 (Student's t-test). (F) Western blot analyses of protein expression of Fgf15, Cyclin D1 and D2 using lysates from NE-4C cells with or without overexpression of miR-302b. β-actin serves as a loading control. (G) Quantification of Western blot data from three independent blots in experiment F. The quantification was determined by densitometry and normalized to β-actin. *P<0.05 (Student's t-test). (H) Relative position of the miR-302 target site in the Fgf15 3′-UTR. Conserved seed region of miR-302a-d (2-8 nt from 5′ of miRNA) are shown in red text, and their alignment with the sequence from Fgf15 3′-UTR is shown. Mutations in the 3′-UTR of Fgf15 (highlighted in black) were introduced to disrupt the base-pairing between miR-302 seed sequences and Fgf15 3′UTR. (I) Luciferase reporter constructs containing wild type or mutated Fgf15 3′-UTR sequences were co-transfected with miR-302b mimics into NE-4C cells. 36 hours after transfection, the firefly luciferase activity was normalized to activity of Renilla. Error bars represent SEM of three replicates for each condition. One way ANOVA

analysis in conjunction with Tukey's test was conducted (*P<0.05); the differences between lane 4 and lane 1 or 2 were not significant.

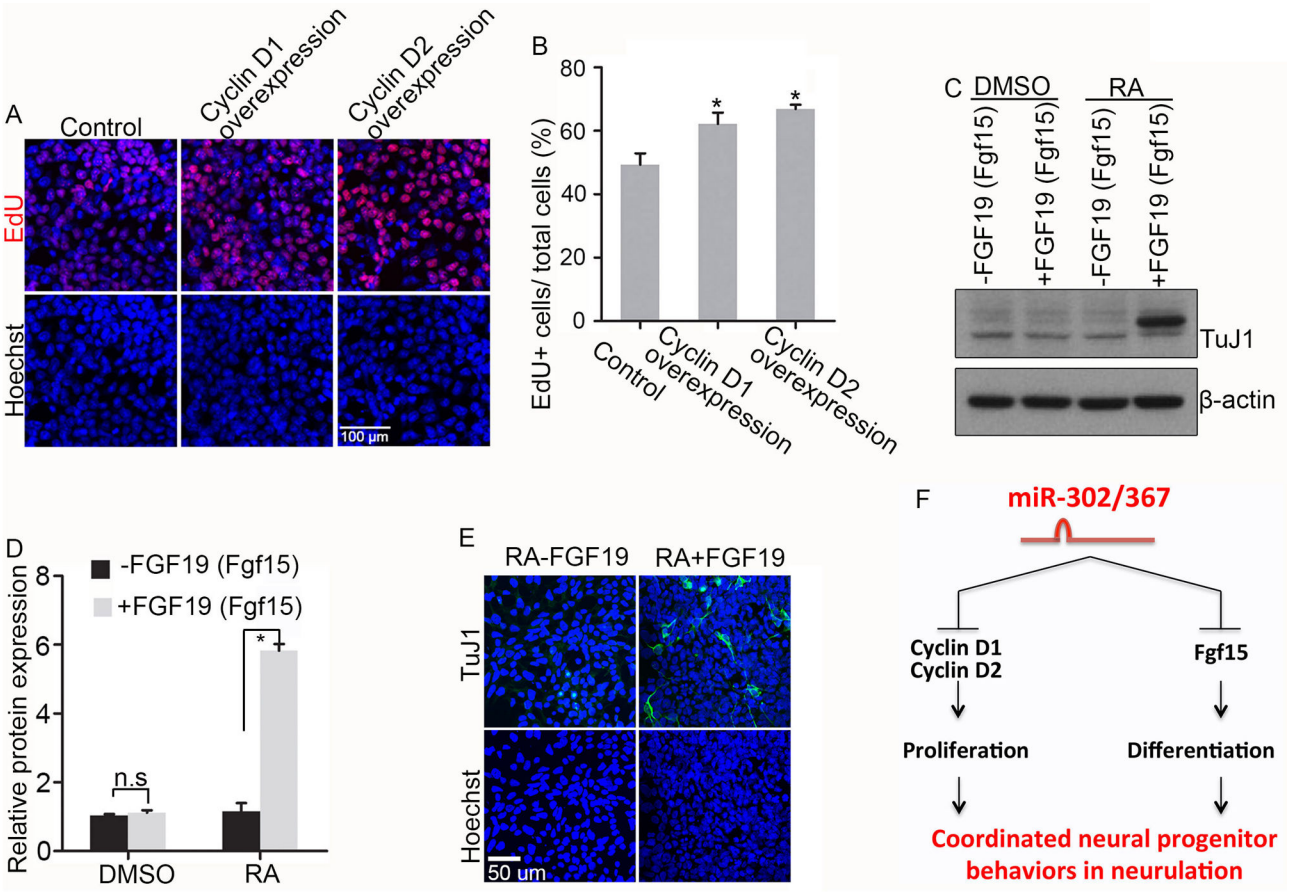

Figure 7.

Effects of overexpression of CyclinD1/D2 and FGF19 on NE-4C cell proliferation and differentiation. (A) Confocal microscope images of NE-4C cells after 25 minute EdU (red) pulse labeling with or without overexpression of Cyclin D1 or D2. Hoechst stains nuclei (blue). Scale bar: 100 um. (B) Quantitative measurement of EdU-positive cells in experiment A. The EdU-positive percentage was calculated as the percentage of EdU-positive cells out of the total numbers of counted NE-4C cells. Error bars represent SEM of three independent experiments, counting more than 2000 cells in each experiment. One way ANOVA analysis in conjunction with Tukey's test was conducted (*P<0.05); the difference between lane 2 and lane 3 was not significant. (C) Western blot analyses of protein expression of TuJ1 using lysates from NE-4C cells with or without treatment of FGF19 (human orthologous of mouse Fgf15 protein). β-actin serves as a loading control. (D) Quantification of western blot data from three independent blots in experiment C. The quantification was determined by densitometry and normalized to β-actin; n.s represents not significant and *p< 0.01 (Student's t-test). (E) Confocal microscopy analysis of TuJ1 expression (green) in retinoic acid (RA) treated NE-4C cells with or without FGF19. Hoechst stains nuclei. Scale bar: 50 um. (F) A working model for the roles of miR-302/367 in neural progenitor cells (NPCs). MiR-302/367 inhibits NPC proliferation by repressing Cyclin D1/D2, and prevents the premature differentiation of NPCs via inhibiting Fgf15 during neurulation.